Hydrogen Bonding and the Inductive Effect in Crystalline and Solution Phases of Hexylamine:$LiCF_3SO_3$ and Dipropylamine:$LiCF_3SO_3$: Application to Branched Poly(ethylenimine)

Nathalie M. Rocher, Roger Frech,* and Masood Khan

Department of Chemistry and Biochemistry, University of Oklahoma, Norman, Oklahoma 73019

Received: June 3, 2005; In Final Form: July 22, 2005

Raman and infrared spectroscopy were used to study the nature of hydrogen bonding and the cation inductive effect in solutions of $LiCF_3SO_3$ dissolved in hexylamine, a primary amine, and dipropylamine, a secondary amine. Comparison of pure hexylamine and hexylamine dissolved in CCl_4 established that the Raman band maximum of the symmetric stretching mode, $\nu_s(NH_2)$, in pure hexylamine originates in molecules undergoing no hydrogen bonding interactions. The addition of $LiCF_3SO_3$ to hexylamine or dipropylamine shifts the frequencies of the solvent NH stretching modes by two effects: the breaking of hydrogen bonds and the cation inductive effect. Comparison of the infrared and Raman spectra allows (to some degree) the separation of these two effects. During these studies, crystalline compounds of hexylamine:$LiCF_3SO_3$ and dipropylamine:$LiCF_3SO_3$ were discovered, and their structures were solved by single-crystal X-ray diffraction techniques. Vibrational spectra of these crystals and detailed structural knowledge of the cation−solvent interactions complement analogous spectroscopic studies of the solution phases. The cation−polymer and hydrogen bonding interactions of branched poly(ethylenimine) (BPEI) complexed with $LiCF_3SO_3$ were modeled by the solutions of hexylamine and dipropylamine containing dissolved $LiCF_3SO_3$. Specifically, lithium ion interactions with the primary and secondary amine groups in BPEI were modeled by the solution studies with hexylamine and dipropylamine, respectively. The analysis of the hexylamine system was particularly useful because the primary amine group of BPEI dominates the NH stretching region of the spectrum.

1. Introduction

Salts dissolved in high molecular weight polymers have been the object of intensive research for a variety of applications, including electrolytes in rechargeable lithium batteries.[1] Much of this research has focused on poly(ethylene oxide) and related polymers.[2−5] The oxygen heteroatoms in the chain can coordinate metal cations, providing a mechanism for the dissolution of the salt in the host polymer matrix. Recent work has considered host polymers with nitrogen as the chain heteroatom, e.g. poly(ethylenimine) and poly(*N*-methylethylenimine).[6,7] However, the relatively low room-temperature conductivities (10^{-7} to 10^{-8} S cm^{-1}) of electrolytes based on these and the PEO-based materials[8−10] have stimulated studies of factors important in understanding ionic conductivity, such as cation−host and cation−anion interactions.[11−15] These studies have been greatly enhanced by examining the structure and dynamics of these interactions in small model compounds whose structures mimic local structures found in the higher molecular weight systems.[16−20]

Although this body of work has important technological implications, the study of cation−host molecule interactions is of fundamental interest in its own right, with relevance to the area of coordination chemistry. Small molecular hosts and polymer hosts with ion-coordinating sites that are also hydrogen bonded present a complex challenge. In these systems, vibrational spectroscopy is a powerful tool for analyzing cation−host interactions as salt is added to the system, although the simultaneous presence of the cation inductive effect and alterations in the hydrogen bonding greatly complicate the interpretation of the observed spectrum.

This paper describes a comparative study of cation−solvent interactions in lithium triflate solutions, $LiCF_3SO_3$ (abbreviated LiTf), with a primary amine, hexylamine (HEXA), and a secondary amine, dipropylamine (DPA). A comparison of the infrared and Raman spectra of the pure components combined with the concentration-dependent measurements of the salt solutions is especially useful in separating the cation inductive effect from the effect of hydrogen bonding. During the course of this study, crystals of hexylamine:LiTf and dipropylamine:LiTf were isolated, and their structures were solved by single-crystal X-ray diffraction methods. Unambiguous knowledge of the local structure present in the crystalline phases (e.g., structural details of the cation−heteroatom interaction and hydrogen bonding interactions) combined with the recognition of similar spectral signatures in concentrated salt solutions provides additional insight into the nature of the interactions. Finally, these interactions are also examined in branched poly(ethylenimine), BPEI, a polymer that has primary, secondary, and tertiary amine groups present.

2. Experimental Methods

2.1. Sample Preparation. BPEI (number average molecular weight = 10 000), hexylamine, dipropylamine, lithium trifluoromethane sulfonate, $LiCF_3SO_3$ (LiTf), sodium trifluoromethane sulfonate, $NaCF_3SO_3$ (NaTf), and tetrabutylammonium triflate (TbaTf) were obtained from Aldrich. The BPEI, hexylamine, dipropylamine, and TbaTf were used as received. The LiTf and NaTf were dried under vacuum at 120 °C for 48 h before use.

* Email: rfrech@ou.edu. Tel: 405-325-3831. Fax: 405-325-6111.

10.1021/jp052965g CCC: $30.25
Published on Web 10/19/2005

Methanol was dried by distilling over sodium metal. The chemicals were stored and used in a dry argon atmosphere glovebox (VAC, ≤1 ppm H_2O) at room temperature. All polymer:salt solutions were prepared by dissolving weighed amounts of BPEI and salt in dry methanol and stirring for approximately 24 h to ensure a homogeneous solution before casting as films. The hexylamine:salt solutions and the dipropylamine:salt solutions were prepared by mixing directly weighed amounts of salt and solvents. The solutions were stirred for a minimum of 24 h before use. The compositions of the samples are reported as a nitrogen-to-cation ratio ($N:M^+$).

Crystals of HEXA:LiTf and DPA:LiTf were grown by leaving solutions in the glovebox at room temperature for a long period of time (6 months). The HEXA:LiTf crystals were white (clear under the microscope) and grainy, and seemed to form out of the highly concentrated solutions first (5:1, 10:1). The entire sample was composed of crystals, with no solution left in the vial. The DPA:LiTf crystals grew as clear needles that formed more rapidly in the less concentrated solutions (30:1, 40:1). After the crystals appeared, no solution was present in the vial. The crystals were then placed in X-ray oil in the glovebox to proceed with the X-ray measurements.

2.2. FT-IR and FT-Raman Spectroscopy. The BPEI:salt samples for FT-IR studies were made by casting the solutions directly onto zinc selenide windows and drying at room temperature under argon for 24 h. The samples were then dried under vacuum at room temperature for an additional 24 h to ensure solvent removal. The hexylamine and dipropylamine:salt solutions were placed between zinc selenide windows in a sealed sample holder; the crystalline samples were ground with potassium bromide and pressed into thin pellets. Infrared data were collected using a Bruker IFS66V FT-IR spectrometer (KBr beam splitter) under vacuum (11 mbar) for the polymeric and crystalline samples, and under dry air purge for the liquid samples. The data were recorded over a range of 500−4000 cm^{-1} with a spectral resolution of 1 cm^{-1}. The FT-Raman samples were sealed in a thin NMR tube under an argon atmosphere. The data were recorded at a 2 cm^{-1} resolution using a Bruker Equinox 55 equipped with an FRA 106/S system. The 1064 nm line of a Nd:YAG laser was used for excitation.

2.3. Differential Scanning Calorimetry. A 3−5 mg amount of crystalline material was sealed in 40 μL aluminum pans under an argon atmosphere. Thermal data were collected using a Mettler DSC 820 calorimeter under a dry nitrogen purge at heating and cooling rates of 5 °C/min. The thermograms were then analyzed using STAR^e v.6.10 software from Mettler Toledo. Each sample was cycled between 0 and 200 °C twice.

2.4. X-ray Diffraction. Single crystals for X-ray analysis were isolated from the HEXA:LiTf and DPA:LiTf solutions. All the data were collected on a Bruker Apex diffractometer using Mo Kα ($\lambda = 0.71073$ Å). The structures were solved by the direct method using a SHELXTL system, and were refined by full-matrix least squares on F^2 using all reflections. All the non-hydrogen atoms were refined anisotropically. All hydrogen atoms were included with idealized parameters.

Data from the HEXA:LiTf crystal were collected at 86(2) K. The final R1 = 0.050 is based on 2374 "observed reflections" ($I > 2\sigma(I)$), and $wR^2 = 0.155$ is based on all reflections (2600 unique reflections). The C1, C2, and C3 atoms at the end of the hexylamine molecule were modeled using two components, with 50% occupancy for each component because of the presence of some static disorder. For the DPA:LiTf crystal, the data were collected at 100(2) K. The final R1 = 0.088 is based on 2198 observed reflections ($I > 2\sigma(I)$), and $wR^2 = 0.268$ is based on all reflections (2642 unique reflections). The dipropylamine ligand is extensively disordered and was modeled with two components (50% occupancy). However, there are additional minor components that could not be modeled because of unstable refinement. The R1 value of 0.088 and the large peaks in the final difference map are due to the disorder of the dipropylamine ligand. Despite the extensive disorder, the geometry of the molecule is reasonable, and the coordination of the lithium cation is determined unambiguously.

TABLE 1: Structural Data of the HEXA:LiTf Crystal

crystal system	orthorhombic
space group	*Pbca*
temperature (K)	86(2)
a (Å)	8.6035(19)
b (Å)	10.008(2)
c (Å)	28.521(6)
volume (Å^3)	2455.7(9)
Z	4
density (Mg/m^3)	1.391
R1	0.0501
crystal size (mm^3)	0.38 × 0.32 × 0.22

TABLE 2: Coordination Bond Distances for the Lithium Cation

bond	bond length (Å)
O1−Li1	1.945(5)
O2−Li1	1.940(5)
O3−Li1	1.959(5)
N1−Li1	2.049(5)

3. Results and Discussion

3.1. Hexylamine:LiTf System. *3.1.1. Crystal Structure.* The compound hexylamine:LiTf crystallizes in an orthorhombic unit cell in the *Pbca* space group, with four (HEXA:LiTf) asymmetric units in the cell. The packing forms a polymeric two-dimensional network in the *a* and *b* directions, as illustrated in Figure 1, with each lithium ion coordinated to one nitrogen atom from the hexylamine molecule and three triflate oxygen atoms from three different triflate ions (Figure 2). The structural data are summarized in Table 1.

The lithium−oxygen coordination bond distance lies between 1.94 and 1.96 Å, whereas the corresponding lithium−nitrogen distance is 2.049 Å (Table 2). Other nitrogen compounds such as *N*,*N*-dimethylethylenediamine,[21] *N*,*N*,*N*′,*N*′-tetramethylethylenediamine,[22] and hexamethyltriethylenetetramine[23] also form complexes with lithium triflate. The Li−O and Li−N bond distances in those complexes compare very well with those found in the hexylamine:LiTf compound.

The two hydrogen atoms of the NH_2 group in hexylamine form hydrogen bonds with triflate oxygen atoms as illustrated in Figure 2. Each hydrogen atom bonds with an oxygen atom belonging to a different triflate ion. Each oxygen atom of a given triflate ion is coordinated to a different lithium ion. In this crystal structure, the distances between the two hydrogen atoms of the amine group and the two triflate oxygen atoms (d(NH···O)) are 2.49 and 2.51 Å (Table 3), and the N−H−O angles are significantly less than 180° (162.9 and 141.1°), suggesting that hexylamine and lithium triflate form weak hydrogen bonds. The structural details of the hydrogen bonds are shown in Table 3.

DSC measurements showed an onset of melting at 75 °C with a midpoint at 80 °C and an onset of recrystallization at 47 °C with a midpoint at 44 °C.

3.1.2. Vibrational Spectroscopy of Hexylamine and Hexylamine:LiTf. The IR spectrum of pure hexylamine (see Figure

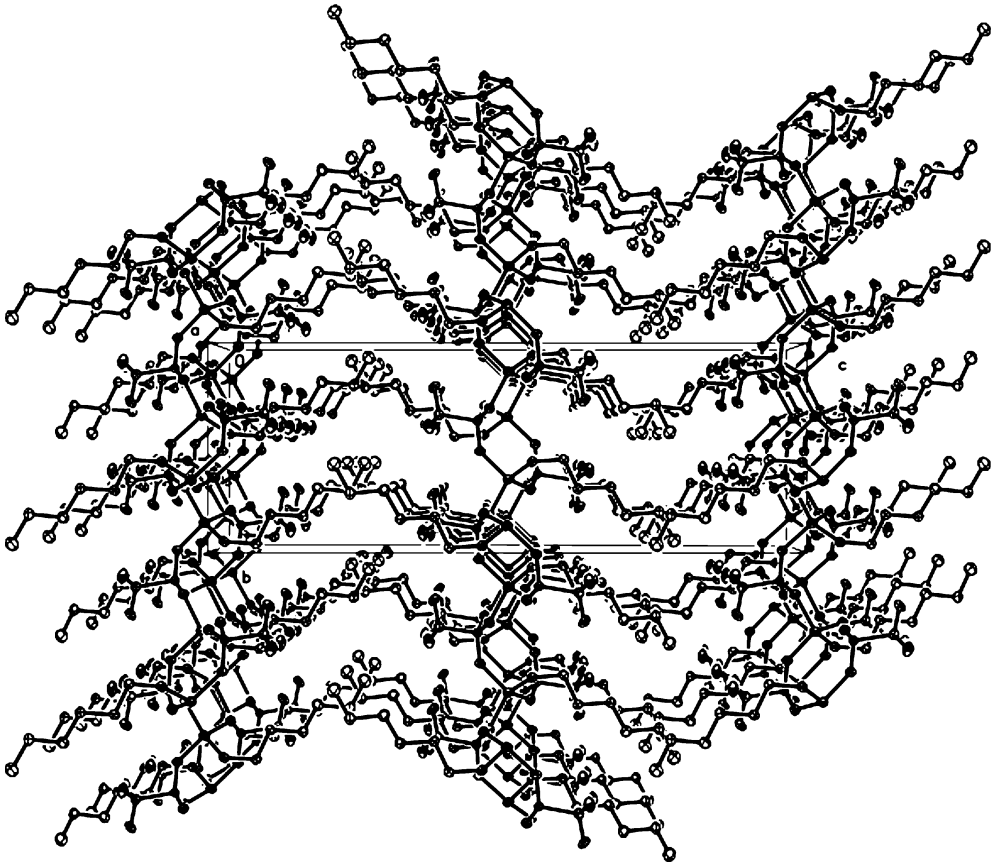

Figure 1. Packing diagram of the hexylamine:LiTf crystal projected down the crystallographic *a* axis. The crystal forms a 2D polymeric structure in the *ab* plane.

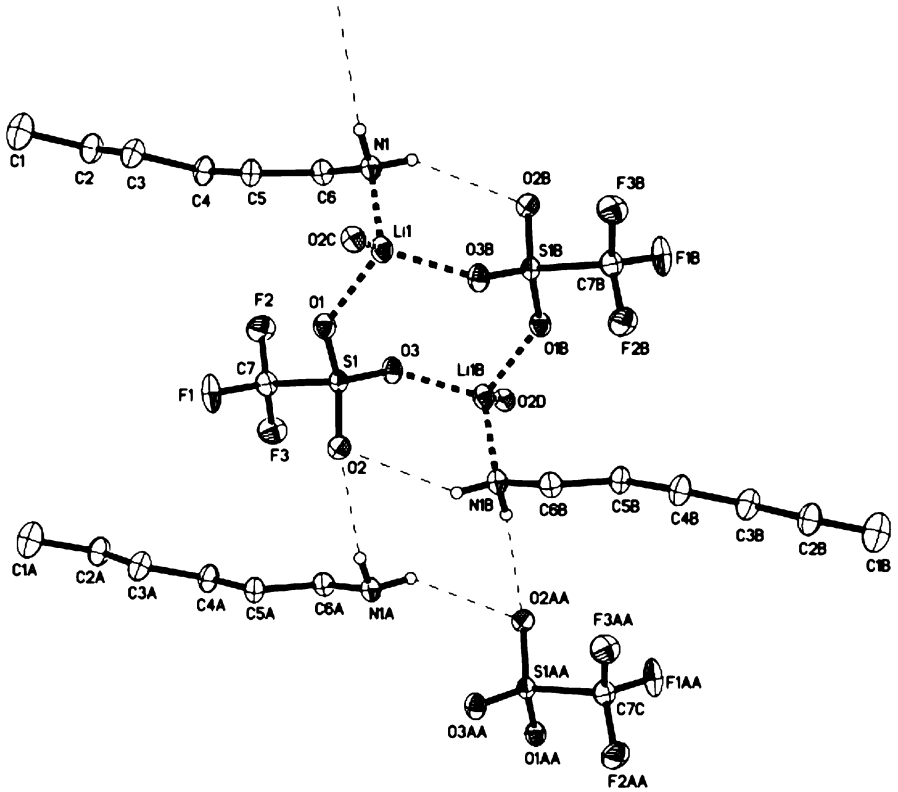

Figure 2. Crystal structure of hexylamine−TiTf showing the 4-fold coordination of lithium and the hydrogen bonding environment of the primary amine group. The disordered part of the hexylamine molecule (atoms C1′, C2′, and C3′) is not shown for the purpose of clarity.

3, lower portion) consists of two strong bands centered at 3371 and 3293 cm^{-1}, corresponding to the antisymmetric NH_2 stretch, $\nu_{as}(NH_2)$, and the symmetric NH_2 stretch, $\nu_s(NH_2)$, respectively. The less intense shoulder centered roughly at 3195 cm^{-1} is an overtone of the NH_2 deformation band at 1609 cm^{-1}. Strictly speaking, the description of the two NH stretching modes of

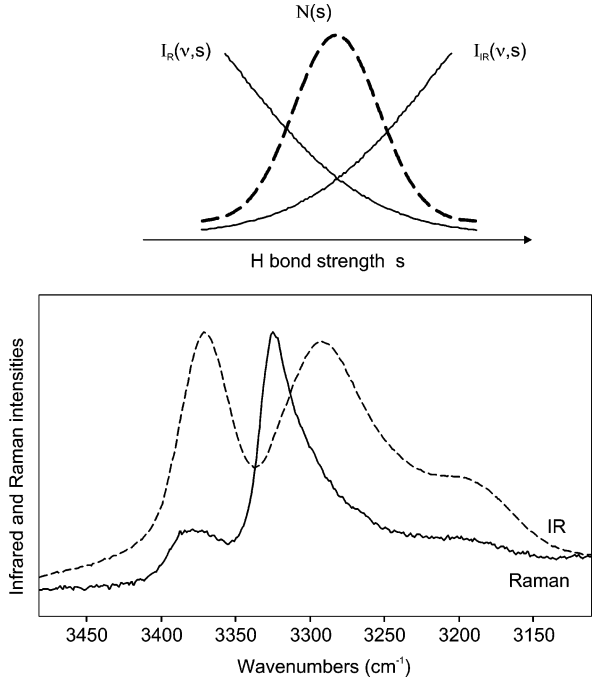

Figure 3. Bottom, IR spectrum (dashed line) and Raman spectrum (full line) of hexylamine in the N−H stretching region. Top, representation of the population distribution of the N−H stretching vibrations in hexylamine as a function of hydrogen bond strength *s*. The corresponding band intensities in IR and Raman are also shown as a function of hydrogen bond strength.

TABLE 3: Hydrogen Bond Parameters for the HEXA:LiTf Crystal

N−H···O	*d*(N−H) (Å)	*d*(H−O) (Å)	*d*(N···O) (Å)	∠(NHO) (deg)
N1−H1E···O2	0.92	2.49	3.376(3)	162.9
N1−H1D···O2	0.92	2.51	3.274(3)	141.1

NH_2 as symmetric and antisymmetric is true for only an isolated NH_2 group or an environment in which the C_{2v} point group symmetry is preserved. In condensed phases, intermolecular interactions usually lower the formal C_{2v} symmetry. However, these labels will be used throughout this paper for reasons of convenience.

The Raman spectrum of pure hexylamine in this region is dramatically different than the IR spectrum. The antisymmetric stretch, centered around 3376 cm^{-1}, has a very weak Raman intensity compared to the symmetric stretch, as expected. The maximum intensity of the symmetric stretch occurs at 3324 cm^{-1}, but a long tail on the low frequency side strongly suggests the presence of hexylamine molecules with a distribution of hydrogen-bonded environments. Hydrogen bonding affects NH stretching frequencies by removing electron density from the N−H bond, causing a shift to lower frequencies.[24,25]

The frequency and intensity data of Figure 3 may be explained in terms of a distribution of hydrogen bonding environments and the following two hypotheses:

(1) The intensity and frequency of the $\nu_s(NH_2)$ mode are quite sensitive to hydrogen bonding interactions because the perturbation of the $\nu_s(NH_2)$ mode by interactions involving one of the amine hydrogen atoms is relatively strong. This arises (in part) because symmetric modes generally have larger Raman scattering cross sections than antisymmetric modes. Assuming that the heteroatom interacts with only one hydrogen atom of the NH_2 group, this interaction necessarily imposes an asymmetric nature on a formerly symmetric mode, thus decreasing the scattering intensity. It is also known that in general the infrared intensity of a hydrogen stretching mode increases with increasing hydrogen bond strength, with a corresponding decrease of Raman scattering intensity. These trends are summarized on the figure by a plot of the Raman intensity $I_R(\nu, s)$ and the infrared intensity $I_{IR}(\nu, s)$ as a function of the hydrogen bond strength, s.

(2) The intensity of the $\nu_{as}(NH_2)$ mode is less sensitive to hydrogen bonding than the $\nu_s(NH_2)$ mode. If the heteroatom involved in hydrogen bonding interacts with only one hydrogen atom of the NH_2 group, the perturbation of the $\nu_{as}(NH_2)$ mode is relatively small because the mode already has a markedly antisymmetric or asymmetric nature.

Also shown in Figure 3 is a population distribution of hexylamine molecules plotted as a function of hydrogen bond strength as indicated. The actual distribution is not known, and this form has been hypothesized for purposes of discussion. In the picture, the $\nu_{as}(NH_2)$ vibrations of all NH_2 groups occur over a small distribution of frequencies, since the frequency of this mode is relatively insensitive to hydrogen bonding. Consequently, the maxima of the IR band (3371 cm^{-1}) and the Raman band (3376 cm^{-1}) are almost coincident. Further, the Raman scattering intensity of this mode is significantly smaller than the intensity of the band at 3324 cm^{-1} that originates in the $\nu_s(NH_2)$ vibration of the NH_2 groups in a weak hydrogen bonding environment. When simple primary amines are dissolved in carbon tetrachloride, thereby eliminating intermolecular hydrogen bonding interactions, measurements of $\nu_s(NH_2)$ result in frequencies close to the value of the hexylamine band at 3324 cm^{-1}. For example, in a very dilute solution of HEXA dissolved in carbon tetrachloride, $\nu_s(NH_2)$ is observed at 3325 cm^{-1} and $\nu_{as}(NH_2)$ at 3392 cm^{-1}. In a dilute CCl_4 solution, the HEXA molecules are effectively isolated from each other and the frequencies are not shifted by hydrogen bonding. As a check, the $\nu_s(NH_2)$ frequency of benzylamine in dilute CCl_4 was also measured at 3325 cm^{-1}. In the absence of hydrogen bonding, the $\nu_s(NH_2)$ vibration has a more truly symmetric nature, and the Raman scattering intensity reflects this situation. In Figure 3, the Raman intensity of the symmetric mode decreases with decreasing frequency as the strength of the hydrogen bonding interactions increases and the mode becomes more antisymmetric in character. At the same time, the infrared intensity of the mode grows until its maximum at 3293 cm^{-1}, as seen in the figure.

The effect of adding salt to hexylamine is illustrated in Figure 4, which shows the IR and Raman spectra of hexylamine:LiTf in the N−H stretching region. Upon the addition of LiTf to bring the solution to a 3:1 composition, both the $\nu_s(NH_2)$ and $\nu_{as}(NH_2)$ bands become sharper in the infrared spectrum. The antisymmetric band shifts lower by 14 wavenumbers (3357 cm^{-1}), whereas the symmetric band shifts higher by 6 wavenumbers (3299 cm^{-1}). In the crystalline sample, the peaks are similarly shifted; $\nu_{as}(NH_2)$ and $\nu_s(NH_2)$ occur at 3358 and 3300 cm^{-1}, respectively. Moreover, a large decrease in the infrared intensity of the symmetric stretch compared to that of the antisymmetric stretch is observed in the crystalline sample. The band shapes of the two stretching modes are slightly distorted in the crystalline sample, with both bands showing a high-frequency tail and a slight but distinct minimum on the low-frequency side. This is a particle-size effect that originates in a reflective scattering contribution to the intensity loss. It is most pronounced when the particle size is on the order of the wavelength of the incident radiation, and both the real and

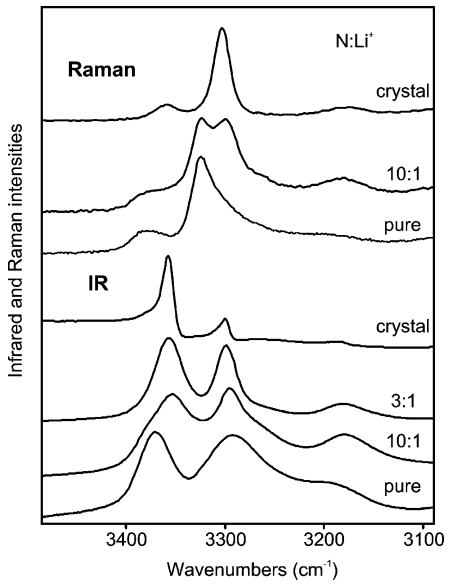

Figure 4. N−H stretching region of the IR and Raman spectra of HEXA:LiTf crystal, hexylamine:LiTf solutions with various $N:Li^+$ ratios, and hexylamine.

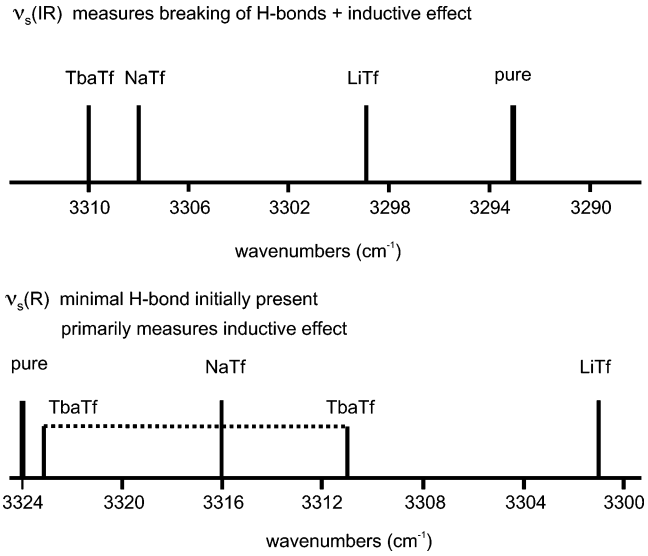

Figure 5. Summary of the NH_2 symmetric stretch frequencies of hexylamine and of the 3:1 $N:M^+$ solutions of hexylamine:LiTf, hexylamine:NaTf, and hexylamine:TbaTf in the IR (top scale) and Raman (bottom scale) spectra.

imaginary parts of the refractive index contribute to the intensity of transmitted light.[26]

Equally dramatic spectral changes with increasing LiTf concentration are seen in the Raman spectra. With the addition of salt, a band at roughly 3300 cm^{-1} grows out of the extensive low-frequency wing of the 3324 cm^{-1} hexylamine band. This is clearly visible in the spectrum of the 10:1 sample. At the same time, the intensity of the 3324 cm^{-1} hexylamine band decreases until it vanishes in the spectrum of the crystal. The weaker Raman-active band at 3376 cm^{-1} in pure hexylamine shifts to 3357 cm^{-1} in the crystal, with no significant change of intensity. In the crystalline compound, the N−H stretching frequencies of the IR and Raman bands are coincident within experimental error. The differences in the intensities of $\nu_{as}(NH_2)$ and $\nu_s(NH_2)$ in the compound can be explained in terms of the crystal structure. In the crystal (see Figure 2), each hydrogen atom of the NH_2 groups is weakly hydrogen bonded to an oxygen atom of a triflate ion, with the hydrogen bonding environment of each amine hydrogen atom roughly equivalent. Therefore, the $\nu_{as}(NH_2)$ and $\nu_s(NH_2)$ modes retain their (approximately) antisymmetric and symmetric nature, respectively, as reflected in the IR and Raman intensities of each mode.

In the LiTf solutions and the crystal, a lithium ion is coordinated to an NH_2 group through the lone pair of the nitrogen atom, which changes the electronic distribution in the NH_2 group. The accompanying decrease of the N−H stretching mode frequencies is known as the inductive effect. The presence of relatively strong hydrogen bonding interactions in pure hexylamine makes it difficult to isolate the inductive effect when LiTf is added. However, it is still possible to draw some conclusions. In pure hexylamine, the $\nu_s(NH_2)$ band at 3324 cm^{-1} was shown to originate in the fraction of hexylamine molecules in which hydrogen bonding was present to a limited extent. The crystal structure (Figure 2) shows that each hydrogen atom of every NH_2 group is weakly hydrogen bonded to an oxygen atom of a triflate ion. Therefore the shift of the 3324 cm^{-1} band of pure hexylamine to 3300 cm^{-1} in the infrared and Raman spectra of the crystal is a reasonable measure of the inductive effect of a lithium ion on $\nu_s(NH_2)$ because of the minimal effect of hydrogen bonding interactions. Unfortunately, it is not possible to carry out a similar analysis of $\nu_{as}(NH_2)$ without knowing how to compensate for the effect of replacing relatively strong N···H hydrogen bonds with significantly weaker O···H hydrogen bonds. However, such a replacement should increase the $\nu_{as}(NH_2)$ frequency. Instead, the frequency decreases from 3376 to 3357 cm^{-1}. Therefore the inductive effect of the lithium ion on the $\nu_{as}(NH_2)$ mode is at least comparable to the effect on the $\nu_s(NH_2)$ mode.

This hypothesis was further tested by spectroscopic measurements of two sets of solutions: NaTf in hexylamine and TbaTf in hexylamine. The pattern of IR and Raman frequency shifts of the symmetric stretch in the two solutions is summarized in Figure 5, along with the previously discussed data for the LiTf solution and pure hexylamine. All salt solutions are compared at a 3:1 molar composition. Tetrabutylammonium is a charge-protected cation; its bulky butyl groups sterically hinder strong interactions with the triflate ion or the nitrogen atom in hexylamine. Consequently, upon addition of tetrabutylammonium triflate salt, it is expected that no inductive effect will take place, and the spectral changes will be due to changes in hydrogen bonding involving the primary amine group.

The data summarized in Figure 5 can be easily understood in terms of the picture introduced earlier. The infrared spectrum preferentially samples those hexylamine molecules whose interactions lead to an asymmetric potential energy environment for the two amine hydrogen atoms. This environment arises because in many of the hexylamine molecules the N···H hydrogen bonds have been broken by nitrogen atom−cation interactions and replaced by O···H hydrogen bonds. The frequency of the observed band is determined by two competing factors: a shift to higher frequencies (breaking of hydrogen bonds) and a shift to lower frequencies (inductive effect). The ordering of $\nu_s(NH_2)$ in the infrared spectra simply reflects the relative strength of the inductive effect for the three cations ($Li^+ > Na^+ > Tba^+$), which accompanies the simultaneous shift to higher frequency that results from hydrogen-bond breaking. By contrast, the Raman spectrum preferentially samples those hexylamine molecules whose amine hydrogen atoms do not undergo hydrogen bonding interactions and therefore experience a relatively symmetric potential energy environment. Therefore the frequency shifts upon complexation with salt simply reflect the strength of the inductive effect, again in the order $Li^+ > Na^+ > Tba^+$.

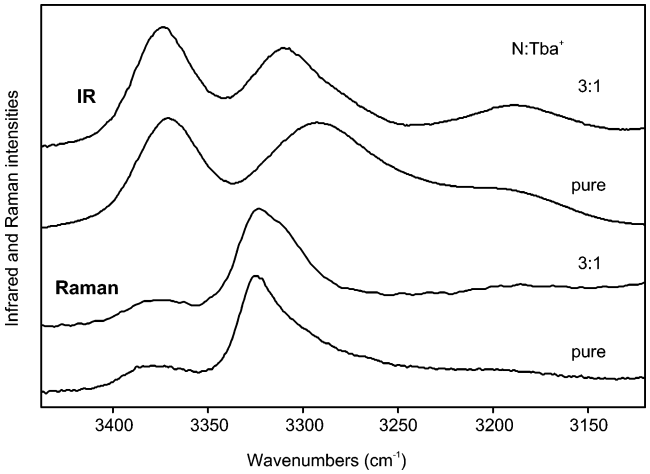

Figure 6. N−H stretching region of the IR and Raman spectra of hexylamine:TbaTf at a 3:1 molar composition and of pure hexylamine.

A comparison of the infrared and Raman spectra of hexylamine with dissolved TbaTf (3:1 composition; see Figure 6) adds additional support to this general picture. The $\nu_s(NH_2)$ band occurs at 3310 cm^{-1} in the infrared spectrum, shifted from the pure hexylamine band at 3293 cm^{-1} as explained above. In the Raman spectrum, there are two clearly discernible $\nu_s(NH_2)$ features: a band at 3323 cm^{-1}, and a very marked shoulder at about 3311 cm^{-1}. The band at 3323 cm^{-1} is essentially due to unshifted hexylamine molecules because of the minimal interaction of the Tba cation with the nitrogen atom. However, in a significant fraction of the hexylamine molecules, the triflate ion oxygen atom forms a hydrogen bond with one of the amine hydrogen atoms, thus shifting the $\nu_s(NH_2)$ band to 3311 cm^{-1}.

3.2. Dipropylamine:LiTf System. *3.2.1. Crystal Structure.* The DPA:LiTf crystals form a monoclinic unit cell in the $P2_1/c$ space group, with four (DPA:LiTf) asymmetric units in the cell. The packing forms a polymeric chainlike one-dimensional network in the *a* direction as illustrated in Figure 7.

Each repeat unit of the network is composed of a $(DPA:LiTf)_2$ dimer that forms the chain via the coordination of lithium to triflate oxygen. In this network, each lithium ion is coordinated to one nitrogen atom from the dipropylamine molecule and three triflate oxygen atoms from three different triflate groups, as shown in Figure 8. Two of these triflate ions belong to the repeat unit of the chain, and the third triflate ion belongs to an adjacent unit. Structural data of the crystal are summarized in Table 4.

The DSC thermograms of the DPA:LiTf crystal showed three endothermic transitions (onset 87 °C, midpoint 99 °C; onset 105 °C, midpoint 120 °C; and onset 99 °C, midpoint 127 °C) that are not reproduced upon cooling and subsequent reheating of the sample. These data suggest that the compound melts incongruently.

The crystal structure shows some static disorder, with each dipropylamine molecule split into two distinct positions of 50% occupancy. In both positions, the lithium−oxygen and lithium−nitrogen coordination bond distances are very similar to that of the hexylamine:LiTf compound (Table 5). The hydrogen atoms of the N1H and N1′H groups are pointing in opposite directions, and therefore have very different environments. Only the N1′H group is shown in Figure 9 for purposes of clarity.

In one of the two positions of the molecule, the hydrogen atom from the N1′H group forms a hydrogen bond with a triflate oxygen from an adjacent plane. These hydrogen bonds are very weak, as the hydrogen−oxygen distance is 3.205(3) Å, and the N1′−H−O angle is 147.1°. In the other position of the dipropylamine molecule, no hydrogen bond is formed.

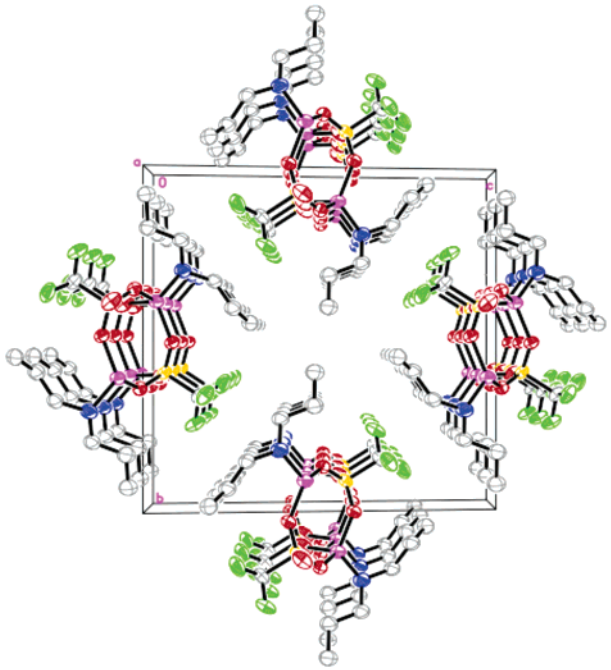

Figure 7. Packing diagram of the dipropylamine:LiTf crystal projected along the crystallographic *a* axis. The stacking of the dimers along the *a* axis forms a polymeric chain.

TABLE 4: Structural Data of the DPA:LiTf Crystal

crystal system	monoclinic
space group	$P2_1/c$
temperature (K)	100(2)
a (Å)	5.1842(4)
b (Å)	15.3790(13)
c (Å)	15.8877(13)
β (deg)	98.1100(10)
volume ($Å^3$)	1254.02(18)
Z	4
density (Mg/m^3)	1.362
R1	0.0490
crystal size (mm^3)	0.34 × 0.28 × 0.18

TABLE 5: Coordination Bond Distances for the Lithium Cation

bond	bond length (Å)
O1−Li1	1.943(3)
O2−Li1	1.934(4)
O3−Li1	1.935(4)
N1−Li1	2.144(4)
N1′−Li1	1.998(4)

3.2.2. Vibrational Spectroscopy. Figure 10 shows the IR and Raman spectra in the ν(NH) region for pure DPA, DPA:LiTf solutions, and the DPA:LiTf crystal. The IR spectrum of pure dipropylamine consists of one weak broad peak centered around 3289 cm^{-1}, whereas the Raman spectrum has two broad weak bands centered at 3327 and 3315 cm^{-1}.

The overall picture of the hydrogen bonding interactions and the inductive effect as illustrated in Figure 3 also provides an explanation for the ν(NH) data of DPA. The interpretation is simplified by having only a single N−H stretching mode for each NH group. Here one might imagine a similar distribution of hydrogen bonding environments, with the Raman intensity being largest for the NH groups with little or no hydrogen bonding, whereas the infrared intensity is greatest for those NH groups undergoing the strongest hydrogen bonding interactions.

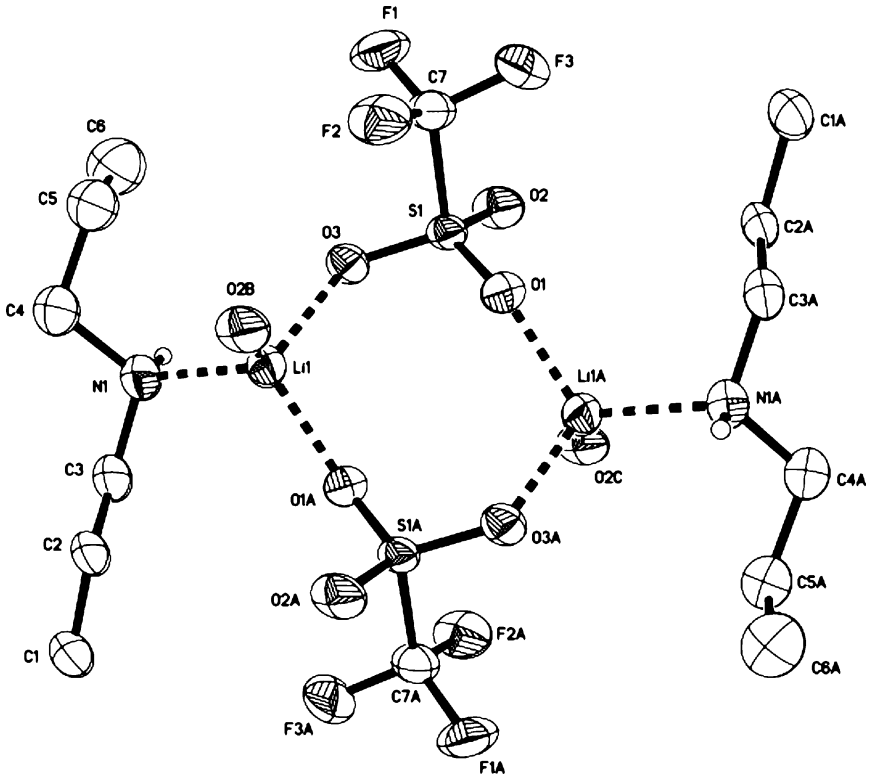

Figure 8. Crystal structure of dipropylamine:LiTf showing one dimer and the 4-fold coordination of lithium. Only one position of the disordered dipropylamine molecule is shown for the purpose of clarity.

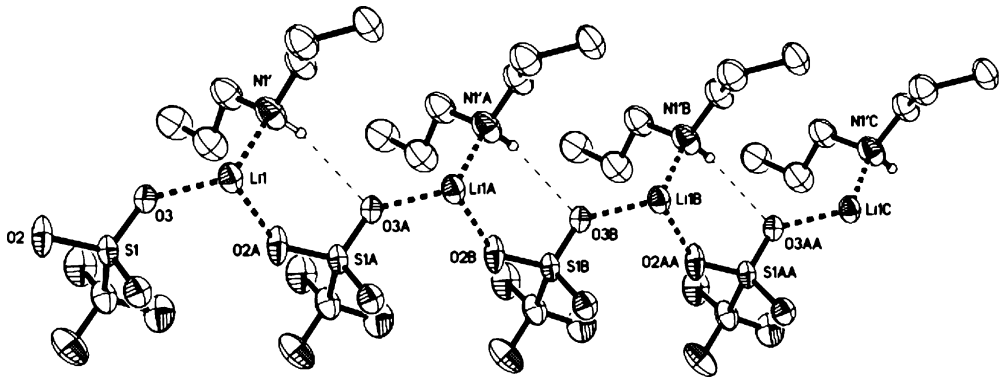

Figure 9. Crystal structure of dipropylamine:LiTf showing the N−H···O hydrogen bonds. Only one dipropylamine is represented; in this view the other molecule would be superposed, with the N−H bond pointing 180° from the illustrated DPA molecule.

The Raman and IR data for the ν(NH) region in DPA, taken together, behave in a manner similar to that of the analogous data for the $\nu_s(NH_2)$ region of hexylamine as described previously. The situation is slightly more complicated in DPA because of the two Raman-active bands at 3327 and 3315 cm^{-1}. This suggests that there are two spectroscopically distinct classes of NH groups in weak hydrogen-bonded environments.

When LiTf is added to DPA, no major shift in the infrared band at 3289 cm^{-1} is observed, but the band becomes sharper until it splits into two distinct peaks at 3302 and 3288 cm^{-1} at the 5:1 composition. The splitting persists in the crystalline sample, with the two peaks observed at 3303 and 3289 cm^{-1}. These two components can be explained with reference to the crystal structure. The static disorder creates two different environments for the hydrogen atom of the NH group. One of the hydrogen atoms is weakly hydrogen bonded to a triflate oxygen, whereas the other hydrogen atom is free. Each band of the ν(NH) region corresponds to one of the two possible positions for the hydrogen atoms in the crystal. The band at 3289 cm^{-1} is assigned to the hydrogen-bonded population, and the band at 3303 cm^{-1} corresponds to the non-hydrogen-bonded population.

In the Raman spectrum, the two bands shift to lower frequency and become two clearly resolved bands in a composition range between 5:1 and 3:1. The spectrum of the crystal is very similar to that of the 3:1 sample, with one band at 3289 cm^{-1} and a weaker band at about 3302 cm^{-1}. This shift to lower frequencies in the Raman spectra was also observed in the Raman spectra of the hexylamine:LiTf system. Unfortunately, TbaTf is insoluble in dipropylamine, and no comparison of cation inductive effects could be made.

3.3. Comparison of ν(NH) in BPEI and the Model Compounds. Because BPEI contains primary, secondary, and tertiary amine groups, the analysis of hydrogen bonding interactions in BPEI is complicated by the numerous kinds of interactions that potentially occur between the groups. The IR and Raman spectra of BPEI in the N−H stretching region are illustrated in Figure 11. In this region, the spectra of BPEI appear

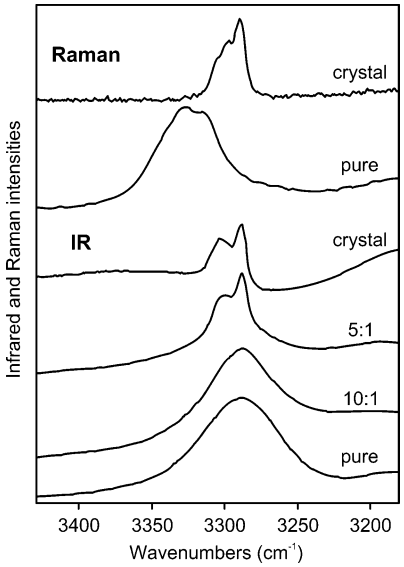

Figure 10. N−H stretching region of the IR and Raman spectra of the DPA:LiTf crystal, dipropylamine:LiTf solutions with various N:Li^+ ratios, and dipropylamine. In this region, the 5:1 Raman spectrum (not shown) is identical to that of the pure solution, whereas the 3:1 Raman spectrum (not shown) is identical to that of the crystal.

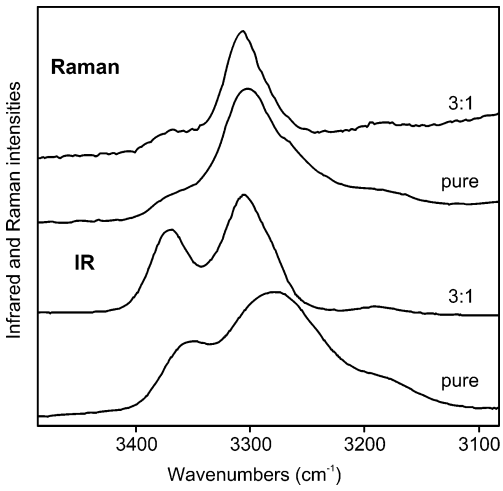

Figure 11. IR and Raman spectra of the N−H stretching vibrations of BPEI and its LiTf complex at a N:Li^+ ratio of 3:1.

to be dominated by the primary amine groups, in part because the vibrational frequency of the secondary amino group in BPEI, ν(NH), overlaps with $\nu_s(NH_2)$ and cannot be distinguished.[27] Therefore a comparison with the NH_2 stretching vibrations in hexylamine is reasonable, although the interactions in BPEI are more complex. In spite of this complexity, it is possible to draw some conclusions.

The strong $\nu_s(NH_2)$ band of the BPEI primary amino group occurs at 3302 cm^{-1} in the Raman spectrum, whereas the corresponding maximum intensity of $\nu_s(NH_2)$ in the infrared spectrum is observed at 3278 cm^{-1}. The shoulder present in both IR and Raman spectra at roughly 3185 cm^{-1} is an overtone of the NH_2 deformation band at 1594 cm^{-1}. The $\nu_s(NH_2)$ Raman band has a weak shoulder at roughly 3266 cm^{-1}, suggesting that there are two groups of hydrogen-bonded NH_2 groups, although they are barely distinguishable via Raman spectroscopy. As in the case of hexylamine, the frequency of $\nu_s(NH_2)$ in the Raman spectrum is higher than its frequency in the infrared spectrum, with a slightly asymmetric lower-frequency wing that extends beneath the infrared-active $\nu_s(NH_2)$ feature. Consequently, the pure BPEI spectra can be analyzed using the same model previously applied to HEXA and DPA, and will not be repeated here. However, there is a significant difference between BPEI and the two model systems that is discussed in the following paragraph.

TABLE 6. Comparison of Frequency Shift Data (cm^{-1}) for BPEI and HEXA Complexed with LiTf at a 3:1 Composition

	$\Delta\nu_s(NH_2)$		$\Delta\nu_{as}(NH_2)$	
	Raman	IR	Raman	IR
BPEI	5	27	18	8
HEXA	−23	5	−21	−14

The N−H stretching bands in the Raman spectrum of BPEI occur at markedly lower frequencies than the corresponding bands of HEXA, i.e., the HEXA → BPEI shift of $\nu_s(NH_2)$ is −22 cm^{-1}, and the $\nu_{as}(NH_2)$ band at 3360 cm^{-1} corresponds to a HEXA → BPEI shift of −16 cm^{-1}. The significantly lower frequencies in BPEI compared with those of HEXA indicate that the NH_2 groups in BPEI are more strongly hydrogen bonded than those in HEXA. In BPEI, there is a high degree of flexibility in both the backbone and side chains, and very reasonable conformations lead to the possibility of strong intramolecular hydrogen bonding interactions in addition to intermolecular hydrogen bonding. The same conclusion is reached when comparing the IR spectra, in which the primary amino group in BPEI gives rise to $\nu_s(NH_2)$ at 3278 cm^{-1} and a weaker $\nu_{as}(NH_2)$ band at 3352 cm^{-1}. These data are similar to those reported by Paul et al.[28] The BPEI frequencies are significantly lower than the analogous modes in hexylamine at 3293 and 3371 cm^{-1}, respectively. It was noted earlier that the secondary amine NH stretching frequency, ν(NH), of BPEI occurs in the same region as the symmetric stretching vibration of the NH_2 group. However, a comparison of the secondary amine NH stretching intensity in the DPA spectrum (Figure 10) with the intensity of the primary amine $\nu_s(NH_2)$ mode in HEXA (Figure 4) shows that the Raman scattering intensity of ν(NH) is much less than that of $\nu_s(NH_2)$. Therefore, conclusions about hydrogen bonding effects on stretching frequencies in these systems based on a comparison of Raman data are more reliable than a comparison of infrared data. Despite this caveat, it is reassuring to see the same trends in the infrared spectra.

The effect of adding lithium triflate to BPEI to a 3:1 composition is also shown in Figure 11. The $\nu_s(NH_2)$ and $\nu_{as}(NH_2)$ bands shift to higher frequencies in both the Raman spectrum (3307 and 3368 cm^{-1}, respectively) and the infrared spectrum (3305 and 3370 cm^{-1}, respectively). These data agree within experimental error with the IR data reported by Paul et al. for BPEI:LiTf at a 4:1 composition.[28] After the addition of salt to bring the composition to 3:1, the band intensity maxima are coincident (within experimental error) in the infrared and Raman spectra, as previously observed in both the hexylamine and DPA solutions. The net effects of adding LiTf to BPEI and to hexylamine to bring the compositions to 3:1 are summarized in Table 6. In the table, the shift $\Delta\nu_s(NH_2)$ is defined as $\nu_s(NH_2$; 3:1 complex) − $\nu_s(NH_2$; pure), with a similar definition for $\Delta\nu_{as}(NH_2)$.

In the Raman spectra, the +5 cm^{-1} shift of $\nu_s(NH_2)$ upon addition of LiTf to BPEI should be contrasted to the −23 cm^{-1} shift in HEXA:LiTf. The $\nu_s(NH_2)$ Raman band in pure BPEI and HEXA results from the NH_2 groups undergoing the least amount of hydrogen bonding, with the Raman band maximum in HEXA originating in NH_2 groups experiencing little or no hydrogen bonding. Therefore, in HEXA the −23 cm^{-1} Raman shift of $\nu_s(NH_2)$ can be attributed almost entirely to the cation inductive effect, although there is a small positive shift

contribution from the formation of weak N−H···O hydrogen bonds with the triflate oxygen atoms. This replacement was pointed out by Paul et al. in BPEI:LiTf.[28] However, in BPEI, the corresponding shift of $+5$ cm^{-1} is presumably due to the partial disruption of hydrogen bonds that are considerably stronger than those in HEXA. As noted before, the coordination of the cation with the nitrogen atom breaks hydrogen bonds, thus increasing the frequency, while the accompanying inductive effect deceases the frequency. In NH_2 groups undergoing significant hydrogen bonding, a weak interaction of the cation with the nitrogen atom would be sufficient to produce a measurable disruption of hydrogen bonding; however, a stronger, coordinative interaction may be required to produce a substantial cation inductive effect. A comparison of the BPEI and HEXA $\nu_{as}(NH_2)$ spectral shifts is informative. In both the Raman and IR spectra, the intensity of the BPEI band increases with salt addition, whereas in HEXA, the intensity of the band decreases. Since the "free" $\nu_{as}(NH_2)$ frequency is about 3392 cm^{-1} in HEXA (from the dilute CCl_4 solution measurement), the large negative shift indicates that the breaking of hydrogen bonds (necessarily a positive shift) is accompanied by a larger negative shift due to the inductive effect. In contrast, the Raman and IR shifts in BPEI $\nu_{as}(NH_2)$ are both positive, suggesting that the strength of the cation interaction with the nitrogen atoms is significantly weaker in BPEI than in HEXA.

3.4. The $\delta(NH_2)$ Band. The frequency of the NH_2 internal bending mode, $\delta(NH_2)$, is also sensitive to hydrogen bonding interactions, although the NH_2 and NH bending modes have not been as well-studied as the stretching modes. Consequently, it is difficult to draw firm conclusions about relative hydrogen bond strengths between different systems from comparative frequency shifts. It is generally understood that the $\delta(NH_2)$ frequency increases with increasing hydrogen bond strength, in contrast to the decrease observed in the N−H stretching frequencies.[24,25] However, the direction of the frequency shift accompanying the cation inductive effect for a bending vibration is not known. In the IR spectrum of hexylamine, there is a broad, asymmetric band centered roughly at 1609 cm^{-1} that decreases with salt addition (1599 cm^{-1} in the 3:1 LiTf complex). The frequency decrease of pure hexylamine with addition of LiTf is due primarily to the breaking of hydrogen bonds and a contribution from the cation inductive effect. The IR spectrum of BPEI contains a broad band at 1594 cm^{-1} that slowly becomes narrower and shifts to higher frequencies with the addition of LiTf (1603 cm^{-1} in the 3:1 complex). This positive frequency increase with the addition of LiTf is discussed in the following section.

4. Conclusions

The infrared and Raman spectra in the NH stretching region of pure hexylamine and pure dipropylamine were shown to selectively sample the population distribution of hydrogen-bonded molecules. In each compound, an NH stretching band was observed in the Raman spectrum with an intensity maximum at a significantly higher frequency than that of the band in the infrared spectrum. This observation was explained by a model in which the Raman spectrum effectively sampled molecules with weak hydrogen bonding interactions, whereas the infrared spectrum sampled molecules with relatively stronger hydrogen bonding interactions.

Studies of HEXA:LiTf solutions and DPA:LiTf solutions were significantly aided by the formation of crystalline compounds whose structures were solved by single-crystal X-ray diffraction methods. In each crystal, the lithium ion is 4-fold coordinated in a similar manner: each lithium ion is coordinated to the nitrogen atom of the amine and to three oxygen atoms from three different triflate ions. In both crystals, the structural data indicate the presence of weak hydrogen bonds between the amine hydrogen atoms and the oxygen atoms of the triflate anion. However, there are no hydrogen bonds between the amine groups of adjacent molecules.

Progressive changes in the IR and Raman spectra with the addition of salt were noted. A spectroscopic comparison of these solution data and corresponding spectra of the two crystals, complemented by knowledge of the two crystal structures, led to a deeper understanding of lithium ion coordination with a primary and a secondary amine group. Frequency shifts observed in the NH stretching region were attributed to a combination of two effects: a change in the hydrogen bonding environment upon addition of salt, as well as the inductive effect of the cation upon coordination to the nitrogen atom. The symmetric NH stretch was shown to be more sensitive to both effects than the antisymmetric stretch. This is due to the fact that the symmetry of the mode is disturbed more readily when a perturbation is applied to it. Moreover, the combination of Raman and IR experiments allowed a separation, to a certain extent, of the contribution from the two effects.

Although the main focus of this paper is on solutions and crystals containing LiTf, the general picture of salt addition effects was further tested by augmenting the LiTf data with spectroscopic measurements of HEXA−NaTf solutions and HEXA−TbaTf solutions. In all three systems, the addition of salt caused a disruption of the hydrogen bonds initially present. Interestingly, the addition of TbaTf appears to have the greatest effect on the HEXA intermolecular hydrogen bonds through the formation of new hydrogen bonds between the triflate oxygen and amine hydrogen atoms. As expected, the inductive effect is in the order LiTf > NaTf ≫TbaTf.

The study of high molecular weight polymers can be greatly aided by comparative studies of small molecules that structurally and functionally mimic parts of the polymer chain. This is a particularly effective strategy for studying ionic coordination in polymers when both the small molecules and the polymer have functional groups that coordinate ions in a similar manner. HEXA and DPA were used to model the primary and secondary amine groups of branched poly(ethylenimine). HEXA was particularly useful for studying hydrogen bonding interactions and the cation inductive effect accompanying the dissolution of LiTf. Extensive comparisons established that the hydrogen bonding interactions in BPEI were significantly stronger than those in HEXA. The strength of the cation interaction with the amine groups was smaller in BPEI, possibly reflecting the tendency toward stronger hydrogen bond formation in BPEI.

In general, the interaction of a cation with the nitrogen atom of an amine that disrupts a hydrogen bond between the nitrogen atom and a nearby amine hydrogen atom would be observed as a positive NH stretching frequency shift. A strong cation−NH_2 interaction would be more effective in disrupting hydrogen bonds, thereby creating a large positive frequency shift. However, a stronger interaction is accompanied by a significant cation inductive effect that would shift the NH stretching frequency to lower values. The observed frequency shift reflects the competition between these two effects. A modest cation−nitrogen interaction results in a net positive frequency shift because the weak inductive effect does not compensate for the disruption of hydrogen bonds. However, a strong cation−anion interaction occurs with a large inductive effect, and the observed frequency shift is negative.

The situation is more complicated for the NH_2 bending modes. The increase of the $\delta(NH_2)$ frequency in BPEI with increasing salt concentration is somewhat surprising because the breaking of hydrogen bonds accompanied by a weak cation inductive effect might be expected to lower the frequency. When LiTf was added to BPEI, the frequency shifts and intensity changes of the Raman and IR bands in the NH stretching region were interpreted as a partial disruption of hydrogen bonds accompanied by a cation inductive effect that was weaker in BPEI than in hexylamine. The problem is understanding the increase of $\delta(NH_2)$ with the addition of salt. The difficulty is that this vibration often contains contributions from other intramolecular motions, e.g. CH_2 scissors and wagging motions. Changing the hydrogen bonding environment may alter the nature of the mode in terms of the admixture of intramolecular motions. Therefore, shifts in $\delta(NH_2)$ are not as reliable as shifts in the NH stretching frequency for drawing conclusions about hydrogen bonding interactions. Further complicating the picture is the lack of knowledge about the direction and magnitude of the $\delta(NH_2)$ frequency shift due to the cation inductive effect. Further work will address these issues.

Acknowledgment. N.M. Rocher thanks the Department of Chemistry and Biochemistry of the University of Oklahoma for its financial support.

Supporting Information Available: Crystallographic information files (CIF) for the crystal structures of hexylamine:lithium triflate and dipropylamine:lithium triflate. This material is available free of charge via the Internet at http://pubs.acs.org.

References and Notes

(1) Armand, M. B.; Chabagno, J. M.; Duclot, M. J. Polyethers as Solid Electrolytes. In *Fast Ion Transport in Solids*; Vashista, P., Mundy, J. M., Shenoy, G. K., Eds.; Elsevier: Amsterdam, 1979; p 131.

(2) Armand, M. *Ionics* **1983**, *9/10*, 745.

(3) Shriver, D. F.; Bruce, P. G. Polymer Electrolytes I: General Principles. In *Solid State Electrochemistry*; 1st ed.; Bruce, P. G., Ed.; Cambridge University Press: Cambridge, 1995; p 95.

(4) Bruce, P. G.; Gray, F. M. Polymer Electrolytes II: Physical Principles. In *Solid State Electrochemistry*, 1st ed.; Bruce, P. G., Ed.; Cambridge University Press: Cambridge, 1995; p 119.

(5) Armand, M. B. *Annu. Rev. Mater. Sci.* **1986**, *16*, 245.

(6) York, S.; Frech, R.; Snow, A.; Glatzhofer, D. *Electrochim. Acta* **2001**, *46*, 1533.

(7) Sanders, R. A.; Snow, A. G.; Frech, R.; Glatzhofer, D. T. *Electrochim. Acta* **2003**, *48*, 2247.

(8) Robitaille, C. D.; Fauteux, D. *J. Electrochem. Soc.* **1986**, *133*, 315.

(9) Munshi, M. Z. A.; Owens, B. B. *Polym. J.* **1988**, *20*, 577.

(10) Sorensen, P. R.; Jacobsen, T. *Electrochim. Acta* **1982**, *27*, 1671.

(11) Johnston, D. H.; Shriver, D. F. *Inorg. Chem.* **1993**, *32*, 1045.

(12) Schantz, S.; Sandahl, J.; Börjesson, L.; Torell, L. M.; Stevens, J. R. *Ionics* **1988**, *28*−*30*, 1047.

(13) Huang, W.; Frech, R.; Wheeler, R. A. *J. Phys. Chem.* **1994**, *98*, 100.

(14) Schantz, S.; Torell, L. M.; Stevens, J. R. *J. Chem. Phys.* **1991**, *94*, 6862.

(15) Frech, R.; Huang, W. *Ionics* **1994**, *72*, 103.

(16) Frech, R.; Huang, W. *Macromolecules* **1995**, *28*, 1246.

(17) Sutjianto, A.; Curtiss, L. A. *J. Phys. Chem. A* **1998**, *102*, 968.

(18) Johansson, P.; Tegenfedlt, J.; Lindgren, J. *J. Phys. Chem. A* **1998**, *102*, 4660.

(19) Rhodes, C. P.; Khan, M.; Frech, R. *J. Phys. Chem. B* **2002**, *106*, 10330.

(20) Rhodes, C. P.; Frech, R. *Macromolecules* **2001**, *34*, 2660.

(21) Rocher, N.; Frech, R.; Khan, M. To be submitted.

(22) Sanders, R. A.; Frech, R.; Khan, M. A. *J. Phys. Chem. B* **2003**, *107*, 8310.

(23) York, S.; Rocher, N.; Frech, R.; Khan, M. To be submitted.

(24) Pimental, G. C.; McClellan, A. L. *The Hydrogen Bond*; W. H. Freeman: San Francisco, 1960.

(25) Jeffrey, G. A. *An Introduction to Hydrogen Bonding*; Oxford University Press: New York, 1997.

(26) Born, M.; Wolf, E.; Bhatia, A. B. *Principles of Optics*, 7th ed.; Cambridge University Press: Cambridge, 1999.

(27) Colthup, N. B.; Daly, L. H.; Wiberley, S. E. *Introduction to Infrared and Raman Spectroscopy*, 3rd ed.; Academic Press: San Diego, 1990.

(28) Paul, J.-L.; Jegat, C.; Lassègues, J.-C. *Electrochim. Acta* **1992**, *37*, 1623.